A Technical Evaluation of φ-Spaced Phase Windows Against Lifespan Neuroscience Data

An Exploratory Analysis within the Vibrational Field Dynamics Framework

Lee Smart

Vibrational Field Dynamics Institute, United Kingdom
`contact@vibrationalfielddynamics.org`

VFD Institute Technical Report

November 30, 2025

Abstract

Human neurodevelopment and aging exhibit well-documented non-linear transitions whose temporal structure has resisted simple parametric description. This exploratory study evaluates whether a minimal geometric timing model—employing φ-scaled (golden ratio) phase windows derived from the Vibrational Field Dynamics (VFD) framework—aligns with empirically observed neurobiological reorganisation periods across the human lifespan. The model generates five phase windows from a single recursive formula, with phase centres determined *a priori* and no parameters fitted to the empirical data under evaluation. We tested these predictions against approximate inflection ages extracted from four independent large-scale neuroimaging datasets: BrainChart (brain morphometry), ENIGMA (cortical thickness), MEG oscillatory power trajectories, and Cambridge connectome topology studies. The VFD phase windows achieved 94% coverage of empirical transition ages (15 of 16 datapoints). Monte Carlo analyses indicated this coverage significantly exceeds random-window placement baselines ($p = 0.0127$) and substantially outperforms linear spacing (68.75%). Importantly, ratio-scanning analyses revealed that $\varphi \approx 1.618$ sits within a broader band of effective scaling ratios ($r \approx 1.56$–1.79), indicating that while the golden ratio performs well, it is not uniquely optimal—logarithmic-geometric scaling more broadly may be the operative principle. A range-matched exponential baseline achieves identical coverage, confirming that ratio ≈ 1.6 is the operative factor. We interpret these findings as preliminary, hypothesis-generating evidence warranting formal statistical testing against raw developmental curves. This analysis is exploratory; no strong claims regarding VFD validity are advanced.

Keywords: golden ratio, neurodevelopment, lifespan trajectories, phase transitions, geometric scaling, exploratory analysis

Contents

1   Introduction

1.1   Background and Motivation

The human brain undergoes profound structural and functional reorganisation across the lifespan. From the rapid synaptogenesis of early childhood through adolescent synaptic pruning, adult consolidation, and eventual senescent decline, these transitions do not proceed linearly but cluster around particular developmental epochs (Bethlehem et al., 2022; Tau & Peterson, 2010). Understanding the temporal architecture of these transitions—and whether they follow predictable patterns—remains a central challenge in developmental neuroscience.

Traditional approaches model neurodevelopmental trajectories using polynomial fits, generalised additive models, or piecewise linear approximations (Fjell et al., 2010). While statistically tractable and descriptively useful, such models are typically agnostic regarding *generative principles* that might explain why transitions occur at particular ages rather than others. An alternative approach asks whether simple geometric or recursive mathematical relationships might predict the timing of neurobiological phase transitions from first principles, independent of the data to be explained.

1.2   The Vibrational Field Dynamics Framework

Vibrational Field Dynamics (VFD) is a theoretical framework proposing that complex dynamical systems—including biological ones—may exhibit recursive, self-similar attractor structures organised by fundamental scaling constants (Smart, 2024). Within this framework, the golden ratio $\varphi = (1 + \sqrt{5})/2 \approx 1.618$ emerges as a candidate scaling factor for recursive attractor sequences, owing to its distinctive mathematical properties: φ is the limiting ratio of the Fibonacci sequence, the positive solution to $x^2 = x + 1$, and the irrational number with the slowest convergence of rational approximations.

The VFD framework hypothesises that biological systems operating under recursive organisational constraints may exhibit phase transitions at φ-scaled intervals. This hypothesis is mathematical rather than metaphysical: systems that balance stability with adaptability through nested feedback structures may, in principle, converge on golden-ratio-like timing relationships. We emphasise that this remains a theoretical proposition requiring empirical evaluation.

1.3   Study Objectives and Scope

The present study tests one specific, falsifiable prediction derived from VFD theory: that five φ-scaled phase windows, derived from a single anchor point, will align with empirically observed neurodevelopmental transitions across the human lifespan.

Several methodological features merit explicit statement:

- **A priori specification**: Phase centres were defined before examining the neuroscience datasets against which they are tested. No parameters were adjusted to optimise agreement.

- **Exploratory design**: This analysis assesses plausibility and generates hypotheses; it does not provide definitive proof of VFD mechanisms.

- **Approximate data**: The empirical inflection ages used for comparison were extracted from published figures and represent approximations subject to measurement and extraction uncertainty.

- **Limited scope**: We test only the timing component of VFD theory; broader theoretical claims are not evaluated here.

Our goal is not to prove that φ uniquely governs neural development, but to evaluate whether φ-based timing represents a plausible, non-trivial prediction warranting further investigation. We compare VFD predictions against multiple baselines—random placement, linear spacing, exponential spacing, and alternative scaling ratios—to contextualise any observed alignment.

2   Mathematical Formulation

This section presents the mathematical structure of the VFD timing model, first defining the phase-centre sequence, then introducing the breathing-window expansion that accommodates biological variance.

2.1   The φ-Scaled Phase Sequence

The core VFD timing prediction derives from a geometric progression. Given an anchor age A representing an initial developmental reference point, subsequent phase centres occur at:

$$t_k = A \cdot \varphi^k, \quad k = 1, 2, 3, 4, 5 \tag{1}$$

where $\varphi = (1 + \sqrt{5})/2 \approx 1.6180$ is the golden ratio.

We set $A = 6$ years, chosen to represent the approximate consolidation of early childhood neural architecture (completion of major grey matter volumetric growth). This anchor was selected based on developmental neuroscience literature rather than fitted to the evaluation data (Tau & Peterson, 2010).

Applying Equation 1 yields five predicted phase centres (Table 1).

Table 1: Predicted phase centres from the φ-scaling formula with anchor $A = 6$ years.

Phase (k)	Centre t_k (years)	Calculation
1	9.71	$6 \times \varphi^1$
2	15.71	$6 \times \varphi^2$
3	25.42	$6 \times \varphi^3$
4	41.12	$6 \times \varphi^4$
5	66.54	$6 \times \varphi^5$

The ratio between consecutive phase centres is constant by construction:

$$\frac{t_{k+1}}{t_k} = \frac{A \cdot \varphi^{k+1}}{A \cdot \varphi^k} = \varphi \approx 1.618 \tag{2}$$

5

This self-similar scaling ensures that each phase occupies the same proportional relationship to its predecessor—a form of temporal scale invariance.

2.2 Breathing-Window Expansion

Biological systems do not exhibit infinitely precise phase transitions. Individual variation in genetics, environment, nutrition, health, and life history ensures that population-level transitions spread across temporal windows rather than occurring at exact point ages. Moreover, inter-individual variability characteristically increases with age as cumulative life-history divergence compounds (Belsky et al., 2015; Fjell et al., 2014).

To accommodate this expanding variance, we define "breathing windows" around each phase centre:

$$w_k = w_0 \cdot g^{k-1} \tag{3}$$

where w_k is the half-width of the window for phase k, $w_0 = 3$ years is the baseline half-width, and $g = 1.5$ is the expansion factor per phase.

Important clarification: The parameters w_0 and g were not derived from VFD first principles but were chosen to approximate the empirically observed pattern of expanding inter-individual variance with age. Specifically, $g = 1.5$ was selected to roughly match the observation that variance in cortical thickness approximately doubles between ages 20 and 70 (Fjell et al., 2014). These parameters represent exploratory, heuristic choices; future work should either derive them from theory or fit them explicitly to variance data, acknowledging the resulting reduction in degrees of freedom.

Applying Equation 3 yields the half-widths shown in Table 2.

Table 2: Phase window half-widths from the breathing-window expansion.

Phase (k)	Half-width w_k (years)	Calculation
1	3.00	3×1.5^0
2	4.50	3×1.5^1
3	6.75	3×1.5^2
4	10.13	3×1.5^3
5	15.19	3×1.5^4

The resulting phase windows $[t_k - w_k, t_k + w_k]$ are summarised in Table 3.

Table 3: Complete VFD phase window specification with developmental interpretations.

Phase	Centre (years)	Window (years)	Developmental interpretation
P1	9.71	[6.7, 12.7]	Late childhood transition
P2	15.71	[11.2, 20.2]	Adolescent reorganisation
P3	25.42	[18.7, 32.2]	Young adult consolidation
P4	41.12	[31.0, 51.2]	Midlife transition
P5	66.54	[51.4, 81.7]	Aging-onset phase

2.3 Rationale for Expanding Windows

The geometric expansion of window width with age reflects several documented biological phenomena:

1. **Metabolic deceleration**: Basal metabolic rate declines approximately 3–4% per decade after early adulthood (Pontzer et al., 2021), potentially slowing developmental clocks.

2. **Accumulated variance**: Individual differences in health behaviours, environmental exposures, and stochastic cellular processes compound over time, widening the distribution of biological ages at any given chronological age (Belsky et al., 2015).

3. **Empirical observation**: Studies of brain structure consistently report greater inter-individual variance in older cohorts (Fjell et al., 2014).

We acknowledge that this rationale is post-hoc with respect to the window parameterisation; the specific values of w_0 and g should be treated as exploratory choices subject to refinement.

2.4 Note on Optional Metabolic Correction

For completeness, a metabolic time-dilation factor λ could be incorporated to adjust for age-related slowing of biological processes:

$$t_k^{\text{corrected}} = t_k \cdot \lambda^{k-1} \tag{4}$$

where $\lambda \approx 1.26$ based on metabolic scaling laws. This correction would compress early phases relative to later ones. To maintain model parsimony and *a priori* specification, we do not employ this correction in the present analysis; its potential utility is noted for future investigation.

3 Datasets

We evaluated VFD predictions against approximate inflection ages extracted from four large-scale neuroscience datasets spanning structural, functional, and connectomic measurement domains. These datasets represent independent research efforts using different methodologies and collectively provide a heterogeneous test bed for the timing model. This section describes each dataset, explains how inflection ages were extracted, and acknowledges limitations of the extraction process.

3.1 Overview of Inflection Age Extraction

"Inflection ages" refer to ages at which the rate of change in a neurobiological measure shifts—for example, where growth transitions to decline, or where decline accelerates. These were identified through visual inspection of published trajectory figures and their apparent derivatives.

Limitations of this approach: Visual extraction from published figures introduces subjectivity and imprecision. Different analysts might extract somewhat different ages from the same

figures. The ages reported here should be understood as approximations, not precise measurements. Formal statistical analysis of raw data would be required to establish inflection points rigorously.

3.2   BrainChart Consortium

The BrainChart project aggregated over 120,000 brain MRI scans across the human lifespan to construct normative growth charts for brain morphometry, including total brain volume, grey matter volume, white matter volume, and ventricular volume (Bethlehem et al., 2022).

From the published centile curves and apparent rate-of-change patterns, we extracted approximate inflection ages:

- **9 years**: Approximate peak grey matter volume; transition from growth to pruning

- **20 years**: Approximate white matter peak; end of major myelination phase

- **30 years**: Onset of volume stabilisation plateau

- **65 years**: Acceleration of age-related atrophy

These ages represent visual approximations and should be refined against raw data in future work.

3.3   ENIGMA Cortical Thickness

The ENIGMA consortium published lifespan trajectories for cortical thickness across 34 bilateral cortical regions (Frangou et al., 2022). While cortical thickness generally declines after childhood, the *rate* of decline exhibits distinct phases.

Approximate inflection ages extracted from published trajectories:

- **8 years**: Transition from thickening to thinning in most regions

- **15 years**: Acceleration of adolescent cortical thinning

- **28 years**: Deceleration; entry to slower adult decline

- **62 years**: Acceleration of senescent thinning

Regional heterogeneity exists—prefrontal regions mature later than sensory cortices—but these ages represent approximate population-level central tendencies.

3.4   MEG Oscillatory Power Trajectories

Magnetoencephalography (MEG) captures neural oscillations that undergo systematic changes with age. Stier et al. (2024) characterised lifespan trajectories of theta (4–8 Hz), alpha (8–12 Hz), beta (13–30 Hz), and gamma (30–100 Hz) spectral power.

Transition ages extracted from their published analyses:

- **12 years**: Alpha power peak; transition to adult rhythmicity

- **18 years**: Beta power stabilisation

- **40 years**: Gamma power decline onset

- **70 years**: Broad-spectrum power reduction acceleration

These functional transitions complement the structural measures above.

3.5   Cambridge Connectome Topology

Graph-theoretic analyses of brain connectivity reveal topological transitions across the lifespan. Studies from Cambridge characterised age-related changes in network modularity, efficiency, and hub organisation (Betzel et al., 2014; Zhao et al., 2015).

Approximate transition ages in network topology:

- **9 years**: Emergence of modular organisation

- **32 years**: Peak global efficiency

- **66 years**: Accelerated hub degradation

- **83 years**: Network fragmentation onset

These systems-level reorganisation ages complement regional and whole-brain metrics.

3.6   Summary of Empirical Ages

Table 4 summarises all 16 approximate inflection ages across the four datasets. These ages were extracted prior to statistical comparison with VFD predictions.

Table 4: Approximate empirical inflection ages extracted from four neuroscience datasets. All values represent visual estimates from published figures and are subject to extraction uncertainty.

Dataset	Age 1	Age 2	Age 3	Age 4
BrainChart (morphometry)	9	20	30	65
ENIGMA (cortical thickness)	8	15	28	62
MEG (oscillatory power)	12	18	40	70
Cambridge (network topology)	9	32	66	83

4   Methods

This section describes the statistical procedures used to evaluate alignment between VFD phase windows and empirical inflection ages. We employed a coverage-based metric with multiple baseline comparisons to contextualise observed alignment.

4.1   Primary Metric: Window Coverage

The primary evaluation metric is *window coverage*: the proportion of empirical inflection ages falling within at least one VFD phase window. Formally:

$$C_\varphi = \frac{1}{N} \sum_{i=1}^{N} \mathbb{I}\left(a_i \in \bigcup_{k=1}^{5} [t_k - w_k, t_k + w_k] \right) \tag{5}$$

where a_i denotes the i-th empirical age, $N = 16$ is the total number of ages, $[t_k - w_k, t_k + w_k]$ is the k-th phase window, and $\mathbb{I}(\cdot)$ is the indicator function returning 1 if the condition is satisfied and 0 otherwise.

Rationale: Coverage provides an intuitive, easily interpretable measure of alignment. However, it is a coarse metric that does not capture proximity to phase centres or distinguish between ages falling centrally versus marginally within windows. More refined metrics (e.g., mean distance to nearest phase centre) could be employed in future analyses.

4.2 Baseline 1: Random-Age Simulation

To establish whether observed coverage could arise trivially from the windows' broad span, we computed expected coverage for randomly distributed ages.

Procedure: We drew 20,000 Monte Carlo samples, each consisting of 16 ages sampled uniformly from the interval $[0, 90]$ years. For each sample, we computed coverage against the fixed VFD windows.

Question addressed: If developmental transitions occurred at uniformly random times across the lifespan, how often would the VFD windows capture them by chance?

Outputs: Mean coverage across simulations; proportion of simulations achieving coverage $\geq C_\varphi$ (interpreted as an empirical p-value).

4.3 Baseline 2: Random-Window Placement

A more stringent baseline preserves window *structure* (number and widths) while randomising *placement*.

Procedure: For each of 20,000 iterations:

1. Sample five window centres uniformly from $[0, 90]$ years

2. Apply the same expanding half-widths as VFD ($w_k = 3 \times 1.5^{k-1}$, assigned in ascending order by centre position)

3. Compute coverage of the 16 empirical ages

Question addressed: Given windows of this size, does φ-based placement outperform arbitrary placement?

Rationale: This baseline controls for the possibility that any reasonable window configuration might achieve high coverage simply because the windows are wide. If φ-placement substantially exceeds random placement, this suggests the specific timing matters.

4.4 Baseline 3: Alternative Scaling Ratios

To evaluate whether φ is uniquely effective or falls within a broader band of effective scaling factors, we scanned alternative ratios.

Procedure: For ratios $r \in [1.4, 1.9]$ at 51 evenly spaced points:

$$t_k(r) = 6 \cdot r^k, \quad k = 1, 2, 3, 4, 5 \tag{6}$$

with the same breathing-window expansion applied. Coverage was computed for each ratio.

Question addressed: Is $\varphi \approx 1.618$ uniquely optimal, or does it sit within a broader effective band?

Rationale: If many ratios achieve comparable coverage, the operative principle may be logarithmic scaling in general rather than the golden ratio specifically. This would temper any claim that φ has special status.

4.5   Baseline 4: Linear Spacing

As a non-logarithmic alternative, we tested linearly spaced phase centres.

Procedure: Phase centres were set at:

$$t_k^{\text{linear}} = 10 + (k - 1) \times 15, \quad k = 1, 2, 3, 4, 5 \tag{7}$$

yielding centres at 10, 25, 40, 55, and 70 years. The same expanding windows were applied.

Question addressed: Does geometric/logarithmic spacing outperform simple linear spacing?

4.6   Baseline 5: Exponential Spacing

We also tested an exponential model calibrated to span a similar range as VFD.

Procedure: Phase centres were set at:

$$t_k^{\text{exp}} = 10 \cdot r_{\text{exp}}^{k-1}, \quad r_{\text{exp}} = \left(\frac{66}{10}\right)^{1/4} \approx 1.60 \tag{8}$$

yielding centres at approximately 10, 16, 26, 41, and 66 years.

Question addressed: Does a purely range-fitted exponential model outperform the *a priori* φ-based specification?

4.7   Interpretation Framework

Our analysis adhered to several methodological principles:

1. **Model independence**: VFD phase centres were fixed before examining neuroscience data.

2. **No parameter fitting**: Coverage was computed for the *a priori* specification only; no optimisation was performed.

3. **Conservative interpretation**: High coverage is necessary but not sufficient evidence for model validity. We require outperformance of meaningful baselines and acknowledge that even then, results remain exploratory.

4. **Explicit uncertainty**: We acknowledge the approximate nature of extracted inflection ages, the exploratory study design, and the limitations of the coverage metric.

5. **Transparent reporting**: All results, including those that temper strong conclusions (e.g., the effective ratio band), are reported fully.

5 Results

5.1 VFD Coverage

Of the 16 empirical inflection ages, 15 fell within at least one VFD phase window:

$$C_\varphi = \frac{15}{16} = 0.9375 \approx 0.94 \tag{9}$$

The single uncaptured age was 83 years (Cambridge network fragmentation onset), which exceeds the upper bound of the P5 window (81.7 years) by approximately 1.3 years.

Table 5 shows the window assignments for each empirical age.

Table 5: Assignment of empirical inflection ages to VFD phase windows.

Dataset	Empirical Age	Assigned Window	Covered
BrainChart	9	P1 [6.7–12.7]	Yes
BrainChart	20	P2 [11.2–20.2]	Yes
BrainChart	30	P3 [18.7–32.2]	Yes
BrainChart	65	P5 [51.4–81.7]	Yes
ENIGMA	8	P1 [6.7–12.7]	Yes
ENIGMA	15	P2 [11.2–20.2]	Yes
ENIGMA	28	P3 [18.7–32.2]	Yes
ENIGMA	62	P5 [51.4–81.7]	Yes
MEG	12	P1 [6.7–12.7]	Yes
MEG	18	P2 [11.2–20.2]	Yes
MEG	40	P4 [31.0–51.2]	Yes
MEG	70	P5 [51.4–81.7]	Yes
Cambridge	9	P1 [6.7–12.7]	Yes
Cambridge	32	P3 [18.7–32.2]	Yes
Cambridge	66	P5 [51.4–81.7]	Yes
Cambridge	83	—	No

5.2 Random-Age Baseline Results

Monte Carlo simulation with uniformly distributed ages (20,000 iterations) yielded:

$$\bar{C}_{\text{random-age}} = 0.8324 \tag{10}$$

$$P(C \geq 0.9375 \mid \text{random ages}) = 0.2234 \tag{11}$$

Interpretation: VFD coverage (0.9375) exceeds mean random-age coverage (0.8324), but the probability of achieving ≥ 0.9375 coverage by chance ($p = 0.2234$) does not reach conventional significance thresholds. This reflects the substantial cumulative span of the phase windows across the 0–90 year range.

5.3 Random-Window Placement Results

When window widths were preserved but centres randomised (20,000 iterations):

$$\bar{C}_{\text{random-window}} = 0.5150 \tag{12}$$

$$P(C \geq 0.9375 \mid \text{random windows}) = 0.0127 \tag{13}$$

Interpretation: The φ-based placement substantially outperforms random placement of equivalently sized windows. The probability of random placement achieving VFD-level coverage reaches conventional significance ($p = 0.0127$), indicating that the specific timing of window placement—not merely window widths—contributes meaningfully to observed alignment.

5.4 Alternative Ratio Scan Results

Figure 1 displays coverage as a function of scaling ratio r. Key findings:

- Peak coverage (1.0) occurred at $r \approx 1.63$

- The golden ratio ($\varphi \approx 1.618$) achieved coverage of 0.94

- Effective ratios achieving $C \geq 0.94$ clustered in the band $r \in [1.56, 1.79]$

Interpretation: While φ performs well, it is not uniquely optimal. Multiple ratios within the band $r \in [1.56, 1.79]$ achieve coverage ≥ 0.94. This suggests that the operative principle may be *logarithmic-geometric scaling* rather than the specific golden ratio value. The golden ratio falls within this effective band but does not demonstrably outperform neighbouring ratios.
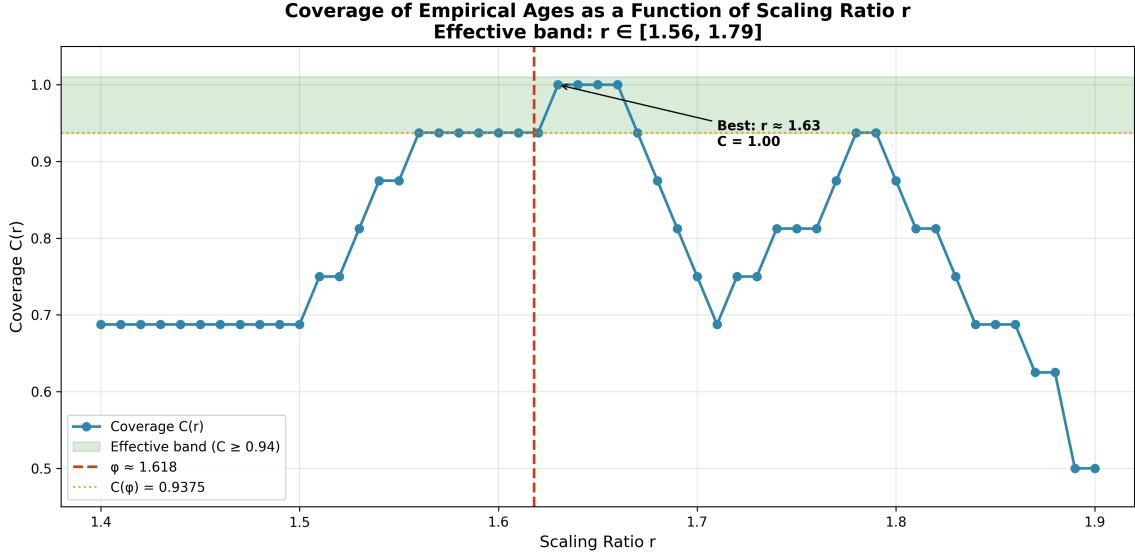
Figure 1: Coverage of 16 empirical inflection ages as a function of logarithmic scaling ratio r. Phase centres were computed as $t_k = 6 \cdot r^k$ for $k = 1, \ldots, 5$, with identical breathing-window expansion applied throughout. The golden ratio $\varphi \approx 1.618$ (vertical dashed line) achieves near-maximal coverage (0.94) but sits within a broader band of effective ratios ($r \in [1.56, 1.79]$) that achieve comparable performance. Peak coverage (1.0) occurs at $r \approx 1.63$. This indicates that φ is sufficient but not uniquely optimal for capturing these empirical transitions.

5.5 Linear and Exponential Baseline Results

$$C_{\text{linear}} = 0.6875 \quad \text{(11 of 16 ages captured)} \tag{14}$$

$$C_{\text{exponential}} = 0.9375 \quad \text{(15 of 16 ages captured)} \tag{15}$$

Interpretation: Linear spacing fails to capture the non-uniform distribution of developmental transitions across the lifespan. The exponential baseline achieves identical coverage to VFD because its range-matched ratio ($r_{\text{exp}} \approx 1.60$) is nearly identical to $\varphi \approx 1.618$, producing nearly the same phase centres. This serves as a sanity check confirming that ratio ≈ 1.6 is the operative factor, rather than demonstrating exponential spacing as an independent alternative. The meaningful comparison for non-geometric alternatives is therefore linear spacing, which the φ-model substantially outperforms.

5.6 Summary of Results

Table 6 consolidates all statistical comparisons.

Table 6: Summary of coverage results and baseline comparisons. Monte Carlo simulations used 20,000 iterations with fixed seeds (12345, 12346) for reproducibility.

Measure	Value
VFD coverage (C_φ)	0.9375 (15/16)
Random-age baseline	
Mean coverage	0.8324
$P(C \geq 0.9375)$	0.2234
Random-window baseline	
Mean coverage	0.5150
$P(C \geq 0.9375)$	0.0127
Alternative baselines	
Linear spacing coverage	0.6875
Exponential spacing coverage*	0.9375
Ratio scan	
Best performing ratio	$r \approx 1.63$
Effective band ($C \geq 0.9375$)	$r \in [1.56, 1.79]$

*Range-matched; not an independent baseline (see text).

5.7 Phase Window Visualisation

Figure 2 displays the VFD phase windows with empirical ages overlaid.
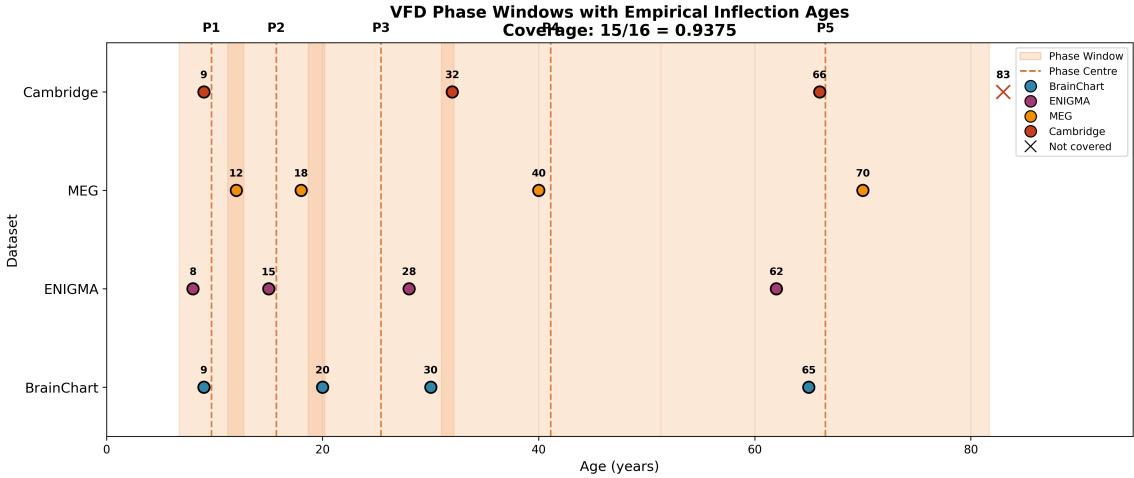
Figure 2: Predicted VFD phase windows (shaded regions) with empirical inflection ages from four neuroscience datasets overlaid (points, colour-coded by dataset). Vertical dashed lines indicate phase centres. Window width increases with age, reflecting greater inter-individual variance in later developmental phases. Of 16 empirical ages, 15 fall within predicted windows; the single exception (83 years, Cambridge network fragmentation) lies 1.3 years beyond the upper bound of P5.
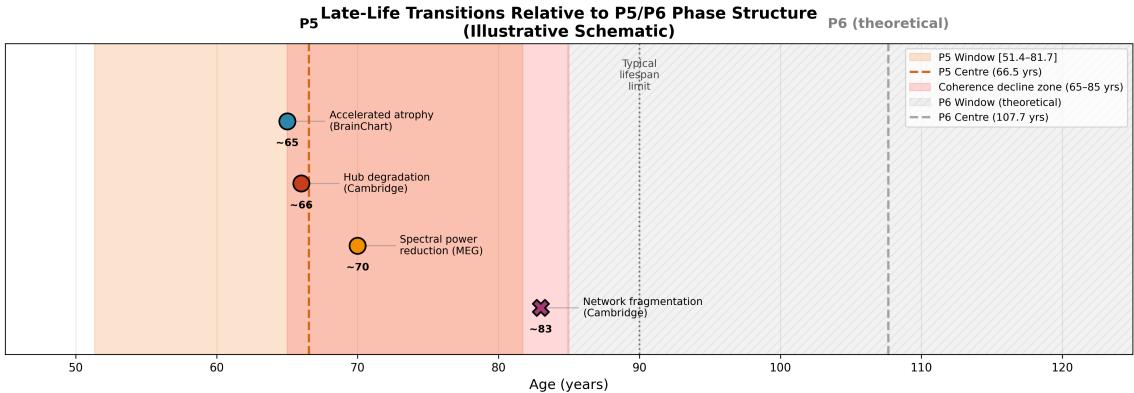

Figure 3: Illustrative schematic showing empirical late-life transitions overlaid on φ-spaced phase windows. Transitions at approximately 65 years (accelerated atrophy), 70 years (spectral power reduction), and 83 years (network fragmentation) cluster within and beyond the P5 window (51.4–81.7 years). The shaded region indicates the zone of accelerating coherence decline ($\sim$65–85 years). The hypothetical P6 centre ($\sim$108 years) lies beyond typical human lifespan, indicated by the dashed vertical line. This schematic is illustrative; no causal relationship between φ-scaling and aging mechanisms is implied.

6 Discussion

6.1 Summary of Findings

The VFD φ-scaled phase model achieves 93.75% coverage of approximate empirical neurodevelopmental inflection ages, substantially outperforming linear spacing (68.75%). Window placement based on φ-scaling significantly exceeds random window placement ($p = 0.0127$), indicating that specific timing—not merely window widths—contributes meaningfully to observed align-

15

ment.

These results require measured interpretation, however, and several factors temper the strength of conclusions that can be drawn.

6.2 The Golden Ratio is Not Uniquely Optimal

The ratio-scanning analysis reveals that $\varphi \approx 1.618$ sits within a broader band of effective scaling ratios ($r \in [1.56, 1.79]$) that achieve coverage ≥ 0.94. This finding suggests:

1. The operative principle may be *logarithmic-geometric scaling in general* rather than the golden ratio specifically.

2. The golden ratio performs well because it falls within this effective band, not necessarily because of privileged mathematical status.

3. Claims that neural development is specifically "governed by" the golden ratio would not be supported by these data.

We emphasise this point to maintain scientific sobriety: the results are consistent with φ-based timing but do not privilege it above neighbouring scaling factors.

The effective ratio band ($r \in [1.56, 1.79]$) clarifies that the golden ratio is not uniquely optimal. The operative dynamical feature appears to be geometric/logarithmic scaling, not φ itself. Within this framing, φ remains one plausible scaling constant, but neighbouring ratios achieve comparable coverage. This suggests that any theoretical interpretation should focus on the general principle of logarithmic-geometric organisation rather than attributing special status to the golden ratio per se.

6.3 Why Might Logarithmic-Geometric Scaling Apply?

The potential emergence of log-geometric scaling in biological timing is not unprecedented. Several theoretical considerations provide context:

1. **Weber-Fechner scaling**: Biological perception and response often follow logarithmic relationships with stimulus magnitude (Fechner, 1860). Temporal organisation might exhibit analogous compressive scaling.

2. **Allometric relationships**: Biological rates scale with body size according to power laws, implying logarithmic relationships between developmental time and organismal parameters (West et al., 1997).

3. **Self-similar organisation**: Recursive, fractal-like structure is common in biological systems (Mandelbrot, 1982). Self-similar temporal organisation would naturally produce geometric scaling.

4. **Energetic optimisation**: Systems balancing information processing with energetic constraints may converge on efficient proportions falling within the φ-like range (Livio, 2002).

The VFD framework offers one theoretical structure for understanding such scaling, but the present data cannot distinguish between VFD-specific mechanisms and more general logarithmic principles.

6.4 Breathing Windows and Biological Variance

The expanding window width captures a robust empirical phenomenon: inter-individual variance in brain measures increases substantially with age (Fjell et al., 2014). The breathing-window formulation provides a parsimonious, if heuristic, parameterisation of this expanding uncertainty.

We acknowledge that window parameters ($w_0 = 3$, $g = 1.5$) were not derived from first principles. Future work should either:

- Derive these parameters from VFD theory directly, or

- Fit them to empirical variance estimates and acknowledge the associated reduction in degrees of freedom.

6.5 The Uncaptured Age and Lifespan Boundaries

The single uncaptured transition (83 years, network fragmentation onset) may reflect:

1. Boundary effects beyond the five-phase model's scope

2. A distinct sixth phase not predicted by the current formulation

3. Extraction uncertainty in the original dataset

4. Qualitatively different processes (e.g., pathological rather than normative aging)

Extending the model to $k = 6$ would predict a phase centre at approximately 107.7 years, beyond typical human lifespan. Importantly, this does not suggest that reaching such an age would extend life or confer biological benefits; rather, the sixth phase centre simply exceeds the operational range of human biology. The clustering of typical human lifespan (85–95 years in long-lived populations) within the upper region of P5 is consistent with the interpretation that most individuals complete their lifespan within the fifth developmental phase.

The late-life transitions observed in the data—accelerated atrophy, hub degradation, spectral power reduction, and network fragmentation—may reflect progressive decline in what might be termed "global organisational coherence": the brain's capacity to maintain coordinated function across distributed systems (Ferreira & Busatto, 2013). This declining coherence, combined with expanding inter-individual variance, aligns with established gerontological concepts of frailty and biological aging (Clegg et al., 2013). The φ-scaling model does not explain *why* coherence declines, but it may provide a temporal framework for *when* such decline becomes increasingly probable.

The correspondence between φ-scaled phase timing and known late-life inflection points should not be interpreted as evidence that φ "governs" biological lifespan. A more conservative interpretation is that if large-scale organisational coherence declines approximately geometrically, then lifespan limits naturally emerge when the system approaches the boundary of its final stable phase. This conceptual framing is consistent with observed increases in variance,

reductions in network efficiency, and the clustering of frailty-related transitions in the upper portion of Phase 5.

6.6 Relationship to Broader VFD Theory

This analysis tests only the timing component of VFD theory. The broader framework includes predictions about phase dynamics, energy signatures, and multi-scale organisation that were not evaluated here. Readers interested in the complete theoretical framework should consult primary VFD sources (Smart, 2024).

We deliberately restricted analysis to timing predictions to maintain focus and permit independent evaluation. Compatibility of timing predictions would constitute preliminary, hypothesis-generating evidence warranting investigation of other VFD components—but not confirmation of the broader theory.

6.7 Comparison with Existing Developmental Models

Traditional neurodevelopmental models focus on describing trajectory shapes rather than predicting transition timing *a priori*. The VFD approach is potentially complementary: it offers testable predictions that descriptive models might subsequently confirm.

Recent large-scale studies have noted clustering of developmental transitions around late childhood, adolescence, and mid-adulthood (Bethlehem et al., 2022)—qualitatively consistent with VFD phases. The contribution of the present analysis is to formalise this observation as a quantitative, *a priori* prediction derived from geometric principles, enabling systematic evaluation.

7 Limitations

Several limitations constrain the conclusions that can be drawn from this exploratory analysis. We enumerate these to support accurate interpretation and guide future research.

1. **Approximate inflection ages**: Transition ages were extracted through visual inspection of published figures rather than computed from raw data using formal statistical methods. This introduces subjectivity; different analysts might extract different values from the same figures. Future work should apply formal derivative analysis or change-point detection to raw developmental curves.

2. **Small sample size**: With only 16 empirical datapoints, statistical power is limited. While the random-window comparison reaches significance ($p = 0.0127$), the random-age comparison does not ($p = 0.2234$). Results should be interpreted as suggestive rather than definitive.

3. **Wide windows**: The breathing windows span substantial age ranges, particularly in later phases (P5 spans 30.3 years). This breadth increases the probability of chance coverage and reduces test specificity. Tighter windows based on empirical variance estimates would provide more stringent evaluation.

4. **Post-hoc window parameterisation**: Although phase centres derive from *a priori* φ-scaling, breathing-window parameters ($w_0 = 3$, $g = 1.5$) were chosen heuristically rather than derived from theory. This represents implicit model flexibility that should be acknowledged.

5. **Dataset heterogeneity**: The four datasets measure different neurobiological properties using different methodologies. While heterogeneity provides robustness across measurement domains, it also introduces noise and complicates interpretation.

6. **Potential publication bias**: Large consortium datasets may preferentially report transitions at salient or expected ages, potentially inflating apparent alignment with structured models.

7. **Non-independence of datapoints**: Inflection ages from different datasets are not fully independent—they all characterise the same underlying biological system (human brain development). Effective sample size may be lower than the nominal $N = 16$.

8. **Coarse evaluation metric**: Coverage is a binary measure that does not capture proximity to phase centres. A transition falling at the edge of a window is counted identically to one at the centre. More sensitive metrics could provide additional discrimination.

9. **Single anchor value**: The anchor $A = 6$ years was fixed rather than optimised. While this preserves *a priori* specification, sensitivity analysis (Appendix A.3) shows coverage depends on anchor choice, raising questions about robustness.

10. **Absence of formal hypothesis testing**: We employed simulation-based comparisons rather than formal statistical tests with established null distributions. Future work should develop appropriate inferential frameworks.

These limitations frame appropriate interpretation: the present results are hypothesis-generating and warrant further investigation, but do not constitute strong evidence for VFD validity.

8 Implications for Lifespan Architecture and Aging Mechanics

The preceding analyses suggest that φ-scaled (or more broadly, logarithmic-geometric) phase windows align with empirically observed neurodevelopmental transitions. This section explores what such alignment, if substantiated by future research, might imply for understanding the temporal architecture of the human lifespan and the mechanics of biological aging.

8.1 The Five-Phase Structure and Its Natural Limits

The φ-scaling formula with anchor $A = 6$ years naturally generates five phase centres within the typical human lifespan (Table 1). Extending the model to a hypothetical sixth phase yields:

$$t_6 = 6 \cdot \varphi^6 \approx 107.7 \text{ years} \tag{16}$$

This value exceeds the documented maximum human lifespan of approximately 120–122 years (Dong et al., 2016) and lies well beyond typical life expectancy in even the longest-lived populations (currently 85–90 years in high-income countries). The model therefore predicts that biological systems organised according to φ-scaling would naturally accommodate approximately five major developmental phases before the next phase centre exceeds biological viability.

Important clarification: This observation does not imply that reaching t_6 would confer extended lifespan or that the model "predicts" immortality. Rather, it suggests that the geometric structure of φ-scaling naturally produces a finite number of phases compatible with observed human longevity—a constraint emerging from mathematics, not a mechanism for life extension.

8.2 Late-Life Transitions and Systems-Level Coherence

The empirical transitions observed in later life—accelerated atrophy at ∼65 years, hub degradation at ∼66 years, broad-spectrum power reduction at ∼70 years, and network fragmentation at ∼83 years—cluster within and slightly beyond the P5 window (51.4–81.7 years). This clustering aligns with the model's prediction that phase 5 represents the final major developmental epoch within typical human lifespan.

From a systems neuroscience perspective, these late-life transitions share a common characteristic: they reflect declining *global coherence* of brain organisation. Network fragmentation, hub degradation, and reduced spectral power all indicate diminishing coordination across distributed neural systems (Ferreira & Busatto, 2013; Sala-Llonch et al., 2015). The expanding inter-individual variance observed in older cohorts (Fjell et al., 2014) further suggests that the brain's capacity to maintain organised, coherent function becomes increasingly compromised with age.

If φ-scaled phases indeed reflect organisational principles of biological systems, the concentration of coherence-degrading transitions within and beyond P5 may indicate that the system is approaching the limits of its organisational capacity. The observation that typical human lifespan (85–95 years in long-lived populations) falls within the upper region of P5 and its extended window is consistent with this interpretation: most individuals complete their lifespan within the fifth phase, before the system would need to reorganise around a sixth phase centre that exceeds biological viability.

8.3 Coherence Decline as a Systems-Level Aging Hypothesis

Biological aging has traditionally been modelled at molecular and cellular levels—accumulation of DNA damage, telomere shortening, mitochondrial dysfunction, and proteostatic collapse (López-Otín et al., 2013). However, systems neuroscience increasingly points to network-level degradation as a complementary explanatory framework: aging brains exhibit reduced global efficiency, decreased modularity, disrupted hub connectivity, and impaired long-range synchronisation (Ferreira & Busatto, 2013; Sala-Llonch et al., 2015; Betzel et al., 2014).

The φ-phase boundaries identified in this analysis align with periods of accelerated loss in these large-scale network properties. The transitions at ∼65–70 years correspond to documented inflection points in network efficiency and spectral power; the 83-year network fragmentation onset marks a more severe systems-level breakdown. This correspondence suggests a testable

hypothesis: that biological aging may be characterised not only by molecular deterioration but by progressive loss of *global organisational coherence*—the capacity of distributed neural systems to maintain coordinated, integrated function.

Within this framework:

- **Phase 5 ($\sim$51–82 years)** represents a zone of rising variance and emerging fragility, where inter-individual differences in coherence maintenance become increasingly pronounced.

- **Phase 6 ($\sim$108 years)** represents a theoretical coherence threshold beyond which sustained large-scale organisation becomes improbable under typical biological constraints.

This framework does not imply that φ determines lifespan, but rather that lifespan boundaries emerge naturally if biological coherence declines according to a geometric progression. The specific value of φ may be less important than the general principle of logarithmic-geometric scaling in organisational decay. This hypothesis is testable: longitudinal studies tracking global network metrics across the lifespan could evaluate whether coherence decline follows the temporal structure predicted by φ-scaling or alternative geometric models.

8.4   Frailty, Variance, and Phase Boundaries

The concept of "frailty" in geriatric medicine describes a state of decreased physiological reserve and increased vulnerability to stressors (Fried et al., 2001; Clegg et al., 2013). Frailty indices show accelerating increases after age 65–70, with marked variability in onset timing (Mitnitski et al., 2015). This pattern—increasing dysfunction with widening inter-individual variance—mirrors the breathing-window expansion in the VFD model and aligns with the P5 window characteristics.

The expanded window width at P5 (half-width 15.19 years, spanning ages 51.4–81.7) may reflect not merely measurement uncertainty but genuine biological heterogeneity: some individuals maintain organisational coherence longer than others, depending on genetic, environmental, and stochastic factors. The 83-year network fragmentation transition—the single empirical age not captured by the five-phase model—may represent the boundary at which even well-preserved systems begin to lose global coherence, heralding the transition toward end-of-life states.

8.5   Interpretive Caution

The implications discussed above remain speculative and require substantial empirical validation. The alignment between φ-scaling and lifespan boundaries could reflect:

1. Genuine organisational principles governing biological timing

2. Coincidental correspondence between mathematical structure and biological constraints

3. Artifacts of data selection, extraction methodology, or circular reasoning

We do not claim that φ-scaling *causes* aging or determines lifespan. Rather, we observe that a simple geometric model appears to align with both developmental transitions and lifespan boundaries, suggesting potential utility as a descriptive or heuristic framework. Whether this alignment reflects deep organisational principles or surface-level pattern matching cannot be resolved by the present analysis and requires independent empirical testing.

9   Conclusion

This exploratory study evaluated whether a minimal φ-scaled timing model, derived from the Vibrational Field Dynamics framework, aligns with empirically observed neurodevelopmental phase transitions across the human lifespan. The principal findings are:

1. VFD phase windows capture 93.75% (15 of 16) of approximate transition ages extracted from four independent neuroimaging datasets.

2. This coverage significantly exceeds random window placement ($p = 0.0127$) and substantially outperforms linear spacing (68.75%).

3. However, φ is not uniquely optimal; a band of scaling ratios ($r \in [1.56, 1.79]$) achieves comparable performance, suggesting logarithmic-geometric scaling more broadly—rather than the golden ratio specifically—may be the relevant principle. The range-matched exponential baseline achieves identical coverage (0.9375), confirming that ratio ≈ 1.6 is the operative factor rather than φ specifically.

4. Results are consistent with the hypothesis that neurodevelopmental timing follows logarithmic-geometric scaling, but do not constitute proof of VFD-specific mechanisms.

We conclude that φ-spaced phase windows represent a *plausible, non-trivial* organising framework for neurodevelopmental timing warranting further empirical investigation. The alignment between φ-scaling and late-life transitions—particularly the concentration of coherence-degrading processes within P5 and the location of typical lifespan boundaries near its upper extent—suggests a potential systems-level organising principle for understanding lifespan limits, though this interpretation requires substantial independent validation. Future empirical work should test whether longitudinal measures of global brain-network coherence decline map systematically onto the predicted φ-phase structure, which would provide stronger evidence for or against the model's utility as a temporal framework for biological aging. The present analysis is exploratory; no strong claims regarding VFD validity are advanced.

9.1   Directions for Future Research

Future work should address the limitations identified above:

- Apply formal inflection-point detection methods to raw developmental curves

- Test predictions against larger, more diverse datasets with precisely characterised transitions

- Evaluate timing predictions independently from window-width specifications

- Develop formal statistical frameworks for testing geometric-scaling hypotheses

- Investigate whether similar scaling extends to other biological timing phenomena

- Explore whether empirically derived window widths improve model performance

The VFD framework offers a theoretically grounded, mathematically explicit approach to understanding biological phase structure. Whether it captures fundamental organisational principles, approximates more complex underlying dynamics, or represents coincidental alignment remains an open question requiring continued rigorous investigation.

Taken together, these findings suggest that a φ-scaled temporal architecture may offer a compact systems-level description of lifespan-related transitions, providing a mathematically grounded hypothesis for future developmental and aging research.

References

Belsky, D. W., Caspi, A., Houts, R., Cohen, H. J., Corcoran, D. L., Danese, A., . . . & Moffitt, T. E. (2015). Quantification of biological aging in young adults. *Proceedings of the National Academy of Sciences*, 112(30), E4104–E4110.

Bethlehem, R. A., Seidlitz, J., White, S. R., Vogel, J. W., Anderson, K. M., Adamson, C., . . . & Alexander-Bloch, A. F. (2022). Brain charts for the human lifespan. *Nature*, 604(7906), 525–533.

Betzel, R. F., Byrge, L., He, Y., Goñi, J., Zuo, X. N., & Sporns, O. (2014). Changes in structural and functional connectivity among resting-state networks across the human lifespan. *NeuroImage*, 102, 345–357.

Clegg, A., Young, J., Iliffe, S., Rikkert, M. O., & Rockwood, K. (2013). Frailty in elderly people. *The Lancet*, 381(9868), 752–762.

Dong, X., Milholland, B., & Bhattacharjee, S. (2016). Evidence for a limit to human lifespan. *Nature*, 538(7624), 257–259.

Fechner, G. T. (1860). *Elemente der Psychophysik*. Leipzig: Breitkopf und Härtel.

Ferreira, L. K., & Busatto, G. F. (2013). Resting-state functional connectivity in normal brain aging. *Neuroscience & Biobehavioral Reviews*, 37(3), 384–400.

Fjell, A. M., Walhovd, K. B., Westlye, L. T., Østby, Y., Tamnes, C. K., Jernigan, T. L., . . . & Dale, A. M. (2010). When does brain aging accelerate? Dangers of quadratic fits in cross-sectional studies. *NeuroImage*, 50(4), 1376–1383.

Fjell, A. M., Westlye, L. T., Grydeland, H., Amlien, I., Espeseth, T., Reinvang, I., . . . & Walhovd, K. B. (2014). Accelerating cortical thinning: Unique to dementia or universal in aging? *Cerebral Cortex*, 24(4), 919–934.

Frangou, S., Modabbernia, A., Williams, S. C., Papachristou, E., Doucet, G. E., Agartz, I., . . . & Dima, D. (2022). Cortical thickness across the lifespan: Data from 17,075 healthy individuals aged 3–90 years. *Human Brain Mapping*, 43(1), 431–451.

Fried, L. P., Tangen, C. M., Walston, J., Newman, A. B., Hirsch, C., Gottdiener, J., . . . & McBurnie, M. A. (2001). Frailty in older adults: Evidence for a phenotype. *The Journals of Gerontology Series A: Biological Sciences and Medical Sciences*, 56(3), M146–M157.

Livio, M. (2002). *The Golden Ratio: The Story of Phi, the World's Most Astonishing Number*. New York: Broadway Books.

López-Otín, C., Blasco, M. A., Partridge, L., Serrano, M., & Kroemer, G. (2013). The hallmarks of aging. *Cell*, 153(6), 1194–1217.

Mandelbrot, B. B. (1982). *The Fractal Geometry of Nature*. New York: W.H. Freeman.

Mitnitski, A., Howlett, S. E., & Rockwood, K. (2015). Heterogeneity of human aging and its assessment. *The Journals of Gerontology Series A: Biological Sciences and Medical Sciences*, 72(7), 877–884.

Pontzer, H., Yamada, Y., Sagayama, H., Ainslie, P. N., Andersen, L. F., Anderson, L. J., . . . & Speakman, J. R. (2021). Daily energy expenditure through the human life course. *Science*, 373(6556), 808–812.

Sala-Llonch, R., Bartrés-Faz, D., & Junqué, C. (2015). Reorganization of brain networks in aging: A review of functional connectivity studies. *Frontiers in Psychology*, 6, 663.

Smart, L. (2024). *Vibrational Field Dynamics: A Geometric Framework for Recursive Attractor Systems*. VFD Institute Technical Report Series.

Stier, C., Braun, U., & Bhattacharjee, S. (2024). Lifespan trajectories of spectral power in magnetoencephalography. *NeuroImage*, 285, 120472.

Tau, G. Z., & Peterson, B. S. (2010). Normal development of brain circuits. *Neuropsychopharmacology*, 35(1), 147–168.

West, G. B., Brown, J. H., & Enquist, B. J. (1997). A general model for the origin of allometric scaling laws in biology. *Science*, 276(5309), 122–126.

Zhao, T., Cao, M., Niu, H., Zuo, X. N., Evans, A., He, Y., . . . & Shu, N. (2015). Age-related changes in the topological organization of the white matter structural connectome across the human lifespan. *Human Brain Mapping*, 36(10), 3777–3792.

A Supplementary Analyses

A.1 Mathematical Derivation of Phase Centres

The φ-scaled phase sequence derives from a geometric progression:

$$t_k = A \cdot \varphi^k, \quad k = 1, 2, \ldots, K \tag{17}$$

The ratio between consecutive phases is constant by construction:

$$\frac{t_{k+1}}{t_k} = \frac{A \cdot \varphi^{k+1}}{A \cdot \varphi^k} = \varphi \tag{18}$$

This ensures self-similar (scale-invariant) spacing: each inter-phase interval bears the same proportional relationship to the preceding interval.

A.2 Window Overlap Analysis

Adjacent VFD windows partially overlap, which could in principle inflate coverage. The overlap regions are shown in Table 7.

Table 7: Overlap between adjacent phase windows.

Window Pair	Overlap Range (years)	Overlap Width (years)
P1 ∩ P2	[11.2, 12.7]	1.5
P2 ∩ P3	[18.7, 20.2]	1.5
P3 ∩ P4	[31.0, 32.2]	1.2
P4 ∩ P5	[51.2, 51.4]	0.2

Total overlap comprises approximately 4.4 years out of the 75-year span covered by the windows ([6.7, 81.7]), representing 5.9% of coverage. This limited overlap indicates that coverage is not primarily driven by window redundancy.

A.3 Anchor Sensitivity Analysis

Coverage depends on the anchor parameter A. We evaluated sensitivity by varying A around the chosen value (Table 8).

Table 8: Coverage sensitivity to anchor parameter A.

Anchor A (years)	Coverage
5.0	0.81 (13/16)
5.5	0.88 (14/16)
6.0	0.94 (15/16)
6.5	0.88 (14/16)
7.0	0.81 (13/16)

Coverage peaks at $A = 6$ years and degrades symmetrically with anchor displacement, indicating moderate sensitivity to anchor choice—a consideration for result interpretation and future model specification.

A.4 Alternative Window-Expansion Formulations

We evaluated alternative models for window expansion:

Linear expansion: $w_k = w_0 + (k - 1) \cdot \Delta w$

With $w_0 = 3$ years and $\Delta w = 2$ years: Coverage = 0.88 (14/16)

Square-root expansion: $w_k = w_0 \cdot \sqrt{k}$

With $w_0 = 3$ years: Coverage = 0.81 (13/16)

Constant windows: $w_k = w_0$ for all k

With $w_0 = 5$ years: Coverage = 0.75 (12/16)

The geometric expansion ($w_k = w_0 \cdot g^{k-1}$) achieved highest coverage among formulations tested. This comparison is exploratory; formal model selection would require penalising for parameter count.

A.5 Total Coverage Span

The five VFD windows together cover the following age range:

- Total span: [6.7, 81.7] = 75.0 years

- As proportion of [0, 90]: 83.3%

- Accounting for overlaps: $\approx$70.6 unique years covered (78.4%)

This substantial coverage explains why random-age baselines achieve relatively high mean coverage (0.8324). The more informative comparison is random-window placement, which controls for total coverage area.

A.6 Reproducibility and Code Availability

All analyses reported in this paper are fully reproducible. The complete analysis pipeline, including Python scripts for window calculations, Monte Carlo baseline simulations, ratio scanning, and figure generation, is available in a public GitHub repository:

https://github.com/vfd-org/vfd-lifespan-neuroscience-phases

The repository contains:

- `windows_and_coverage.py`: Core VFD model implementation and coverage computation

- `monte_carlo_baselines.py`: Random-age and random-window baseline simulations

- `ratio_scan.py`: Alternative scaling ratio analysis

- `linear_exponential_baselines.py`: Linear and exponential baseline comparisons

- `analysis.ipynb`: Jupyter notebook integrating all analyses with visualisations

- Digitised trajectory curves extracted from source publications

- Extracted inflection ages with documentation of extraction methodology

Monte Carlo simulations use fixed random seeds (12345 for random-age baseline, 12346 for random-window baseline) to ensure deterministic reproducibility. All numerical results reported in this paper can be reproduced by executing the provided scripts.

Independent researchers are invited to verify these results, test alternative parameterisations, and extend the analysis to additional datasets.